

# Galaxy Morphologies in the Cluster CL1358+62 at $z=0.33$ <sup>1</sup>

Daniel Fabricant

Center for Astrophysics, 60 Garden St., Cambridge, MA 02138

and

Marijn Franx and Pieter van Dokkum<sup>2</sup>

Leiden University, P.O. Box 9513, NL-2300, Leiden, the Netherlands

*Accepted for publication in the Astrophysical Journal*

## ABSTRACT

We describe the morphological composition of a sample of 518 galaxies in the field of CL1358+62 at  $z=0.33$ , drawn from a large *HST* mosaic covering 53 sq. arcmin. The sample is complete to  $I=22$ , corresponding to  $M_V=-18.5$  in the rest frame. The galaxy morphologies have been independently classified by the authors of this paper and by Alan Dressler. Dressler's classifications place our work in context with the previous MORPHS study, and allow us to estimate the scatter between different sets of visual classifications.

We restrict most of our analysis to the brighter part of the sample,  $I < 21$  ( $M_V < -19.5$ ), where the scatter between the two sets of classifications is  $\sim 1$  in morphological type. The scatter doubles at  $I = 22$ , presumably due to the lower signal-to-noise and poorer sampling of faint, small galaxy images. To  $I=21$  the two sets of classifiers agree on the fraction of early type galaxies (elliptical+S0): 72%. We conclude that CL1358+62 does not contain the large population of spiral galaxies found in other studies of clusters at  $z \sim 0.3$ , and that there is probably a significant spread in the degree of cluster evolution at intermediate redshift.

The two groups of classifiers differ on the relative fraction of S0 and elliptical galaxies. We show that the distributions of ellipticities and bulge/total light cannot resolve this discrepancy. Nonetheless, we can derive significant constraints on physical models for the evolution of the galaxy population in CL1358+62. The higher ratio of S0 to elliptical galaxies (1.6) found by DF/MF/PvD requires that the evolution preserve the relative fraction of elliptical, S0 and spiral galaxies. Alternately, the lower ratio (1.1) found by AD requires that the evolution preserve the early-type to spiral ratio while increasing the S0 to elliptical ratio. In the latter case, a possible evolutionary mechanism is accretion of galaxies that predominantly evolve to S0's between  $z=0.33$  and the present.

We use our large body of spectra to make the correspondence between spectral and morphological type. Our data follow the pattern seen in the field at low redshift:

---

<sup>1</sup>Based on observations with the NASA/ESA Hubble Space Telescope and the W. M. Keck Observatory

<sup>2</sup>Present address: California Institute of Technology, MS 105-24, Pasadena, CA 91125

emission line spectra are more prevalent among the later morphological types. The 11 identified k+a galaxies (absorption line spectra with strong Balmer lines) have S0–Sb morphologies.

## 1. Introduction

The WFPC2 camera on the Hubble Space Telescope (*HST*) has made it possible to determine the morphologies of galaxies at intermediate redshift and beyond. It has been known for some time that the photometric and spectral properties of galaxies in intermediate redshift clusters differ from galaxies in nearby clusters; the population of blue, star-forming galaxies and post-starburst galaxies is larger at intermediate redshift, see e.g., Butcher & Oemler (1984), Dressler (1987), Gunn & Dressler (1988), Couch & Sharples (1987), and Dressler & Gunn (1999). Given the correlation between the spectral and morphological properties of galaxies (Morgan & Mayall (1957), Morgan & Osterbrock (1969), Kennicutt (1992)), we might be able to detect a corresponding evolution of galaxy morphology in intermediate redshift clusters. However, the evolution of morphology is likely to be more subtle than spectral evolution, since galaxies of the same morphological type can have significantly different star formation rates (e.g. Jansen et al. (1999)).

In the most ambitious study of this sort with WFPC2 to date, the MORPHS group have classified over 1200 galaxies in 10 clusters at  $0.37 < z < 0.56$  (Smail et al. (1997)). They find that S0 galaxies are less common than in low redshift clusters and that the ratio of S0's to E's within a radius of  $\sim 600$  kpc (for  $H_0=50$ ,  $q_0=0.5$ ) decreases with redshift, falling from 2 in low redshift clusters to less than 0.5 at  $z = 0.5$ .

Andreon, Davoust & Heim (1997) (see also Andreon (1998)) have independently classified galaxies in a WFPC2 image of Cl0939+4713, one of the less concentrated clusters in the MORPHS sample. They find a ratio of S0's to E's of  $\sim 2$ , quite comparable to a low- $z$  reference sample in the Coma Cluster. However, they classify 40–50% of the galaxies in Cl0939+4713 as spirals (S), in contrast with 20–30% S in a comparable region of the Coma Cluster. The sample of galaxies in Cl0939+4713 is relatively small ( $\sim 70$ ), and redshifts are available for less than one third of these.

Couch et al. (1998) present a study of the morphological types in three clusters at  $z=0.31$ , also using WFPC2 images. There is substantial overlap between the authors of this paper and the MORPHS group, and the two groups have attempted to adopt a consistent morphological system. At  $z=0.31$ , Couch et al. find an excess of S's, with an abundance at small radii ( $\sim 400$  kpc for  $H_0=50$ ,  $q_0=0.5$ ) approximately twice that in low- $z$  reference clusters. However, averaged over the three clusters, within 400 kpc, they find a ratio of S0's to E's at most slightly depressed relative to regions of comparable galaxy surface density in low- $z$  clusters.<sup>3</sup>. Note, however, that the average  $z$  of the MORPHS clusters is larger (0.46).

Lubin et al. (1998) report the morphological types in two more distant clusters at  $z \sim 0.9$ .

---

<sup>3</sup>It is important to account for the morphology-density relation when we consider the morphological content of clusters. At high galaxy densities, typically found in the cores of clusters, the low- $z$  reference population becomes increasingly dominated by E's, Dressler et al. (1997)

One cluster, CL0023+04, appears to be composed of two low velocity dispersion groups, and contains predominantly S's. The other, CL1604+43, with a velocity dispersion of  $\sim 1200$  km s $^{-1}$ , contains  $\sim 76\%$  early-types. In the latter case, the S0/E ratio is found to be  $1.7 \pm 0.9$ . This result is sensitive to the assumed morphological composition of the foreground/background population, but is evidence that the S0/E ratio does not decline smoothly with  $z$ .

Our approach is complementary to the Dressler et al. (1997), Andreon, Davoust & Heim (1997), and Couch et al. (1998) studies which predominantly describe the galaxy morphologies in cluster cores. We use mosaics of WFPC2 fields to study the galaxy population in a larger region (allowing larger galaxy samples per cluster), and we have acquired large numbers of spectra of cluster galaxies. The spectra remove ambiguity about cluster membership and allow us to directly connect the morphological and spectral properties of the galaxies. Our sample of clusters is x-ray selected, with x-ray luminosities exceeding  $4 \times 10^{44}$  erg s $^{-1}$  in the 0.2–4.5 keV band.

In CL1358+62 at  $z=0.33$ , we have drawn a complete sample of 518 galaxies to a magnitude limit  $I=22$  from a WFPC2 mosaic image of CL1358+62 covering 53 square arcminutes. Spectra for 276 of the 518 galaxies in the morphological sample were previously obtained at the Multiple Mirror and William Herschel Telescopes. The color-magnitude relation of the 194 spectroscopically confirmed cluster members in the *HST* mosaic (3 are fainter than  $I=22$ ) has been previously described in van Dokkum et al. (1998). The spectroscopic properties of 232 cluster members (some outside the *HST* mosaic), as well as the cluster dynamics have been described in Fisher et al. (1998).

Our objectives in this paper are fourfold. (1) We introduce the morphological classification techniques that we will apply to our entire sample of clusters. (2) We classify the galaxies in CL1358+62 at  $z=0.33$ , comparing our classifications with those of an experienced external researcher, Alan Dressler. Our deep sample with two independent classifications provides a useful assessment of the scatter between WFPC2 visual morphological classifications at intermediate redshifts. (3) We describe the robust, classifier-independent conclusions and explore the physical implications of the differences between the two sets of classifications. (4) We connect the spectral and morphological types of the cluster galaxies.

The paper is organized in the following fashion. In § 2, we describe the photometric catalog from which the morphological sample was drawn. The two set of morphological classifications are discussed in § 3. The morphological composition of the cluster and evidence for morphological evolution are presented in § 4. The connection between the morphological and spectral properties of the galaxies is made in § 5. § 6 contains a brief discussion and conclusions.

## 2. Photometric Catalog

Our photometric catalog, from which we draw galaxies for morphological classification, is derived from the *HST* F814W mosaic image. The techniques used to construct the mosaic are described in van Dokkum et al. (1998). Our use of the mosaic image, instead of individual WFPC2 CCD frames, slightly compromises the accuracy of the photometry, but considerably simplifies the source detection problem by eliminating most of the boundaries. Because our goal is to select a

sample of galaxies for morphological classification to a consistent magnitude limit, rather than to perform precision photometry, this is a beneficial tradeoff. We used the SExtractor package, described by Bertin & Arnouts (1996), to detect the galaxies and perform the photometry. We use a detection and analysis threshold of 24.5 mag arcsec<sup>-2</sup>, and a zeropoint of 30.546 (3600 s exposures, May 1997 WFPC2 SYNPHOT update) to convert from instrumental magnitudes to a Cousins *I* magnitude<sup>4</sup>. The adopted zeropoint is the average of the value for the 3 WFPC2 CCDs, which vary by  $\sim\pm0.01$  magnitudes. We use the SExtractor total magnitude estimator (see Bertin & Arnouts (1996)), which is insensitive to the analysis threshold.

In order to allow convenient comparisons with the results of the MORPHS group (Dressler et al. (1997)), we calculate a conversion of observed *I* magnitudes (for  $z < 0.6$ ) to a *V* magnitude in the rest frame. Some of the MORPHS classifications used WFPC2 F702W filter data, so we also derive a consistent conversion from F702W magnitudes to a rest frame *V*. The intent in Dressler et al. (1997) was to work to a consistent limit of  $M_V = -20$ , but a transcription error from Table 9 of Holtzman et al. (1995) led to the adoption of a deeper limit of  $M_V \sim -19$ . (Here and throughout we use  $M_V$  to refer to a rest frame *V* absolute magnitude.) In contrast with Dressler et al. (1997), we also apply an evolutionary correction to allow a closer comparison with low  $z$  clusters. We adopt the Dressler et al. (1997) cosmological model ( $H_0 = 50$  km s<sup>-1</sup> Mpc<sup>-1</sup>,  $q_0 = 0.5$ )

We use four numbers in addition to the distance modulus to convert from the WFPC2 magnitudes to  $M_V$ : (1) the conversion from the Vega-referenced WFPC2 natural filter system to Cousins filter bands, (2) the  $z$ -dependent *K* correction to transform the observed Cousins *R* and *I* magnitudes to the rest frame, (3) the estimated rest frame galaxy colors, and (4) a  $z$ -dependent evolutionary correction. Each of these numbers depends on the spectral energy distribution of the galaxies, so the accuracy of this procedure is limited. We use these numbers, however, only to choose sample limiting magnitudes appropriately scaled with  $z$ . We adopt the approximate expressions described below for these conversions.

We first fit a linear relation to the synthetic transformation of F702W to *R* as a function of  $V - R$  (valid for  $V - R < 1.5$ ), using results from Fig. 10 of Holtzman et al. (1995):

$$R - F702W = 0.31(V - R) \quad (1a)$$

We take the  $V - R$  colors of galaxies as a function of  $z$  from Frei & Gunn (1994), with a morphological mix of 70% E and 30% Sbc to convert (1a) to:

$$R - F702W = 0.31(0.5373 - 0.9132z + 10.17z^2 - 11.21z^3) \quad (1b)$$

To a good approximation (0.1 mag), Fig. 9 of Holtzman et al. (1995) shows:

$$I - F814W = 0 \quad (1c)$$

We fit polynomials to the average *K* corrections of Frei & Gunn (1994) and Poggianti (1997), using 70% E and 30% Sbc or Sc contributions:

$$K_R = 0.4293z + 3.807z^2 - 2.903z^3 \quad (2a)$$

---

<sup>4</sup> Throughout the paper we consistently refer to a Cousins *I* magnitude, which is very close to the natural F814W system referred to a Vega zeropoint (Holtzman et al. (1995))

$$K_I = 0.4910z + 0.4836z^2 \quad (2b)$$

From Frei & Gunn (1994) we take:

$$V_{rest} - R_{rest} = 0.53 \quad (3a)$$

$$V_{rest} - I_{rest} = 1.10 \quad (3b)$$

From the the early-type galaxy fundamental plane study of Kelson et al. (1997) we derive an evolutionary correction:

$$EC_{V_{rest}} = -0.77z \quad (4)$$

The corrections are applied in the following fashion:

$$I = M_V + DM + EC_{V_{rest}} - (V_{rest} - I_{rest}) + K_I$$

Here,  $DM$  is the distance modulus. Applying these expressions to CL1358+62, with a distance modulus at  $z = 0.3283$  of 41.62, we find that the MORPHS limit of  $M_V = -20$  corresponds to an observed  $I = 20.5$ .

Our photometric catalog completeness extends below  $I = 23$ , but we have limited our morphological sample to  $I = 22$  to increase the reliability of the morphological classifications. At  $I = 22$ , we attain a signal-to-noise ratio (S/N) that is very similar to the S/N attained at the  $I = 23$  classification limit adopted by the MORPHS group for their deeper images (Smail et al. (1997)). The standard deviation of the sky noise in our (3600 s) CL1358+62 image has an equivalent surface brightness of 24.4 mag arcsec $^{-2}$ , as compared with 25 mag arcsec $^{-2}$  typical for the ( $\sim$ 12600 s) MORPHS images. A crude scaling relation can be derived by assuming that all galaxies have the same surface brightness, and that our criterion is that classifications of equal reliability require the same number of pixels at the same S/N. For a shallower image, we can effectively bin the image of a brighter galaxy that is  $n$  times larger  $n \times n$  pixels to achieve a S/N that is  $n$  times better. To recover a sky S/N deficit of 0.6 mag, we need to set a limit  $\sim$ 1.2 mag brighter.

### 3. Morphological Classification

There are 518 galaxies in the morphological catalog after removing stars and image artifacts. In the rest frame, the filter central wavelength corresponds to  $\sim$ 6100 Å. We use the F814W images for morphological classification because they are deeper than the F606W images. Dressler et al. (1997) have used either F702W and F814W images for classification at comparable redshifts (between 0.37 and 0.41).

Below, we describe two sets of morphological classifications. The first set was carried out by the authors of the paper using the techniques described in §3.1. We realized that our classifications would be of greater value if we could compare them with morphological classifications from an external expert. Alan Dressler (AD) kindly agreed to independently classify the entire sample. Dressler is a member of the MORPHS group, and most importantly, has classified a large reference sample of low- $z$  cluster galaxies. The strength of the AD classifications is that the same

experienced classifier has classified the galaxies at low and intermediate redshifts. Consistency has obvious benefits when searching for evolution.

However, it is important to keep in mind the difficulty of classifying these relatively faint and small galaxies from WFPC2 images. The brighter cluster ellipticals and S0's in CL1358+62 ( $I \sim 19$ ) have effective radii (half-light radii),  $r_e$ , of  $0.5''$  to  $0.6''$ . The faintest galaxies in the sample ( $I \sim 22$ ) have  $r_e \sim 0.3''$ . The 50% encircled energy radius of WFPC2 stellar images measured from our frames is about  $0.17''$ , so the numbers of meaningful information elements are small: typically 20 to 40. For this reason, we cannot be sure that agreement on a common morphological system is the most significant issue. Even the most experienced classifier may not account for all the systematic differences between the low  $z$  (photographic) and the intermediate  $z$  WFPC2 images. By comparing the two sets of morphological classifications we will be able to discern which aspects of the classification are most robust.

### 3.1. DF/MF/PvD Classifications

The 518 sample galaxies were independently classified along the revised Hubble sequence by DF, MF and PvD from  $96 \times 96$  pixel “postage-stamps” drawn from both the mosaic and original individual CCD images. We referred frequently to Sandage (1961) and Sandage & Tammann (1987), as well as to artificially redshifted digital images drawn from the Nearby Field Galaxy Survey (Jansen et al. (1999)). We assigned numerical types as follows: -5 (elliptical), -4 (elliptical or S0), -2 (S0), 0 (S0 or Sa), 1 (Sa), 3 (Sb), 5 (Sc), 7 (Sd), 9 (Sm), 10 (Im) and 99 (peculiar or merger). Intermediate types (2, 4, 6, and 8) were also assigned.

For 80% of the galaxies, the three independent classifications span a range of three or fewer numerical types (we consider -4, -2 and 0 to be adjacent numerical types), and agree exactly for 34% of the sample. For 6% of the sample, the object is considered unclassifiable by one or more of the authors, or else the classifications disagree wildly. In these cases, we assign a numerical type of 999. The remaining 14% are classified type 1 or later by all the authors, but with a broader range of classifications. Table 1 lists the combination rules used to assign types where the agreement is not exact, including type 15 for indeterminate late types.

### 3.2. AD Classifications

Following the completion of the DF/MF/PvD classifications, AD independently classified the CL1358+62 galaxies according to techniques described in Smail et al. (1997). AD does not assign galaxies to the DF/MF/PvD intermediate types -4 (E or S0) or 0 (S0 or Sa) in the same fashion, preferring to subdivide these into E/S0 (-4), S0/E (-3), S0/Sa (-1) and Sa/S0 (0). When discussing the cluster population in broad terms, AD's types -5 and -4 are combined into E, types -3, -2 and -1 into S0, and etc. DF/MF/PvD split the contents of the -4 bin equally into E and S0, and the 0 bin equally into S0 and Sa. When converting AD's descriptive types into numerical types, we have placed a few galaxies into the merger (99) bin where an individual catalog object corresponds to an interacting or merging pair of objects.

Augustus Oemler, another member of the MORPHS group, independently classified 307 galaxies from the CL1358+62 sample ( $I=22$  limit) to check if AD's classifications adhere to the MORPHS system. Oemler's classifications agree very well with AD's overall, with  $\sim 10\%$  more S0's by number, and a corresponding decrease in the numbers of E's. The number of spirals is identical in both classifications.

### 3.3. Quantitative Comparison of the Classifications

Like any measurement, classifications will suffer from random and systematic errors. We can estimate these errors by comparing multiple sets of classifications. Ideally, such a comparison should be based on classifications using independent imaging data. Here, both sets of classifiers (DF/MF/PvD and AD) worked from the same data set, so we may underestimate the errors. Nonetheless, this comparison is quite interesting. Figure 1 shows the difference between DF/MF/PvD and AD morphological types for individual galaxies as a function of magnitude. As expected, the differences increase at fainter magnitudes. To avoid creating artificial gaps in Figure 1, we condensed and shifted the numerical types of the early type galaxies for this presentation: -3 for E's, -2 for E/S0's and S0/E's, -1 for S0's, 0 for S0/Sa and Sa/S0. For types Sa and later, the "normal" types were used. Galaxies which were classified as merger, peculiar, or unclassified by one group were ignored.

Figure 2 is a scatter diagram comparing the two sets of classifications. The scatter is dominated by random differences, but there is some evidence for systematic differences for the early type galaxies. We return to this point below. The scatter between the classifications has been measured by calculating the mean absolute deviation, and normalizing it to the mean absolute deviation of a gaussian with an rms of 1. This measurement of the scatter is much more robust than the RMS of the differences. The result is shown in Figure 3. The scatter is  $\sim 1$  for bright galaxies, but increases strongly faintwards of  $I = 21$ . The appendix describes how classification errors might systematically bias our population estimates; unfortunately we cannot simply calculate correction factors. In what follows, we restrict most of our analysis to the subset of galaxies with  $I < 21$ .

### 3.4. Classification of Ellipticals and S0s

Figure 2 shows a systematic difference in the DF/MF/PvD and AD classifications of early type galaxies. This is not surprising as the division between E and S0 is a difficult problem in visual classifications. We might hope that looking at two objectively determined structural parameters for the galaxies, ellipticity and the bulge/total light ratio, might be helpful in resolving this issue. For example, Smail et al. (1997) compare the ellipticity distributions of the MORPHS E and S0 intermediate- $z$  galaxies with those from an Andreon et al. (1996) study of Coma Cluster galaxies as a consistency check of the MORPHS classifications.

We have therefore examined the structural properties of the CL1358+62 galaxies measured

by the Medium Deep Survey (MDS) group<sup>5</sup>, Ratnatunga, Griffiths & Ostrander (1999). The MDS group has published structural properties for 70% of the CL1358+62 galaxies in our morphological catalog. The missing 30% are located near frame edges or in one mosaic frame that is not yet included in the MDS database. The MDS group has chosen the best fitting of four structural models for the objects in their catalogs: star, disk, bulge, or disk + bulge, accounting for the point spread function of HST. If a galaxy model is chosen, the MDS group fit the ellipticity of the disk, bulge or disk and bulge separately as appropriate. We focus on two structural parameters derived from these fits: the ratio of bulge to total light, and the weighted ellipticity. The ratio of bulge to total light follows trivially from the best fit model, or from the fits to the disk + bulge model. We calculate the weighted ellipticity from the MDS disk and bulge ellipticities, weighting by the fractions of light in the disk and bulge.

In Figures 4 and 5 we plot the distributions of the bulge to total light ratio for the E and S0 galaxies with  $I < 21$  in the DF/MF/PvD and AD samples, respectively. Excepting the differences in numbers, the distributions for both E's and S0's look remarkably similar for the two sets of classifications.

In Figures 6 and 7 we plot the distribution of weighted ellipticities for the same E and S0 galaxies ( $I < 21$ ), again showing the DF/MF/PvD and AD samples independently. Caution must be exercised when comparing to these to other measures of ellipticity since the MDS numbers are corrected for the HST PSF. A larger fraction of the AD E's have ellipticities exceeding 0.2, but the mean AD E ellipticity is 0.22, only slightly larger than the DF/MF/PvD mean of 0.17. The ellipticities of the two samples of S0's are similar: AD finds a mean ellipticity of 0.46 and DF/MF/PvD find a mean ellipticity of 0.40. The sizable difference in the numbers of E and S0 galaxies found by the two sets of classifiers is not reflected in a large difference between the structural parameters for the two samples of E's or S0's. We conclude that although the total number of early-type galaxies is well established, the SO to E ratio in CL1358+62 is uncertain.

#### 4. Morphological Composition of CL1358+62 and Evidence for Evolution

We have learned that the differences between the two sets of classifications rise steeply below  $I = 21$ , suggesting this as a practical limit for our morphological study. This is also conveniently close to the effective limit of our spectroscopic completeness. We have redshifts for 277<sup>6</sup> of the 518 galaxies in the morphological sample, and 191 of these are cluster members by the criteria given in Fisher et al. (1998):  $0.31461 < z < 0.34201$ . The spectroscopic completeness is 89% for the galaxies brighter than  $I = 20.5$  (corresponding to  $M_V = -20$ ), falling to 59% for  $20.5 < I < 21$ , 33% for  $21 < I < 21.5$ , and 9% for galaxies with  $21.5 < I < 22$ .

---

<sup>5</sup>The MDS catalog is based on observations with the NASA/ESA HST, obtained at the STSCI, operated by AURA.

<sup>6</sup>In one case, a spectrum was obtained of a pair of galaxies separated by  $0.7''$ , one (#1295) at  $I = 21.17$  and the other (#1297) at  $I = 20.92$ . We have assigned the measured velocity (cz=99657) to both galaxies. Galaxies #1481 and #1483 may have both fallen within the spectrograph slit. We assign the measured velocity (cz=99792) to #1483, which is 1.2 mag brighter.

Table 2 lists positions,  $I$  magnitudes, both sets of morphological classifications, and radial velocities for galaxies brighter than  $I=21$ .

#### 4.1. Morphological Composition

We may study the morphological composition of the subsample of known members, which is nearly complete to the MORPHS's depth of  $M_V = -20$ , without concern about background galaxy subtraction. The subsample of known cluster members to  $I = 20.5$  (or  $M_V = -20$ , see § 2) contains 138 galaxies. DF/MF/PvD classify  $27\pm4\%$  of these as E,  $44\pm6\%$  as S0,  $29\pm5\%$  as S, with 1 unclassified galaxy. (The errors here and in the following discussions account only for the Poisson statistics of the number of galaxies per classification bin.) AD classifies  $35\pm5\%$  as E,  $38\pm5\%$  as S0, and  $27\pm4\%$  as S. In both cases, the total early type population is  $\sim72\%$ . To  $M_V=-20$ , then, the only difference between the two groups of classifiers is the relative numbers of E's and S0's.

We consider also the complete photometric sample to a depth of  $I = 21$  (or  $\sim M_V = -19.5$ ), where a small background correction is necessary. To  $I = 21$  our sample contains 298 galaxies, for which we have 236 redshifts (79.2% completeness). Of the 236 galaxies with redshifts,  $65\pm8$  are nonmembers, yielding a foreground/background count of  $82\pm10$  after correcting for the spectroscopic completeness. We determine the morphological composition of the foreground/background galaxies directly from our spectroscopic sample, which contains 86 foreground/background galaxies. DF/MF/PvD classify 3% E, 13% S0, 77% S, and 6% mergers. AD classifies 11% E, 9% S0, 71% S, and 9% mergers. We average these classifications, and adopt a background composition of 7% E, 11% S0, 74% S and 8% mergers. For comparison, Dressler et al. (1997) adopt a morphological composition of 10% E, 10% S0, and 80% S.

After correcting for background, to  $I = 21$ , DF/MF/PvD find a population of  $25\pm4\%$  E's,  $46\pm5\%$  S0's,  $29\pm6\%$  S's, and  $0\pm1\%$  mergers. AD finds  $36\pm4\%$  E's,  $36\pm5\%$  S0's,  $28\pm6\%$  S's, and  $1\pm1\%$  mergers. These results are indistinguishable from those for the brighter spectroscopic sample, with  $\sim72\%$  early-types in both sets of classifications.

#### 4.2. Morphological Evolution

We search for morphological evolution in CL1358+62 by comparing its population with that of equivalent low- $z$  clusters. Judging which low- $z$  clusters are equivalent is somewhat uncertain, but we take as an approximation low- $z$  clusters with a similar number of galaxies within a fixed metric aperture, allowing us to correct for the effects of the morphology-density relation. We use the nearby cluster catalog of Dressler (1980), reanalyzed and summarized in Dressler et al. (1997) as a benchmark. We use the subset of high concentration clusters (10 of 55) in the low- $z$  sample for comparison, because CL 1358+62 was selected for its high x-ray luminosity and has a concentration index  $C\sim0.49$  (Fabricant, McClintock & Bautz (1991)).

The data for the 10 high-concentration clusters are plotted in Fig. 12 of Dressler et al. (1997). There are an average of  $\sim63$  cluster galaxies within a radius of 1450 kpc in these clusters to

$M_V=-20.4$ . In CL1358+62, there are  $\sim 114$  cluster members within this radius to  $M_V=-20.4$ , so CL1358+62 is richer than the average cluster in the low- $z$  sample. However, the low- $z$  sample does contain a high-concentration cluster as rich as CL1358+62: the Coma Cluster. Furthermore, the density difference between CL1358+62 and the average low- $z$  reference cluster, 0.3 dex, is comparable to the bin size in the morphology-density relation plots in Dressler et al. (1997).

The comparison between the morphological composition of the CL1358+62 sample to  $M_V=-20$  and the low- $z$  reference sample is made in Table 3 and Figure 8. The DF/MF/PVD S0/E ratio,  $1.6 \pm 0.3$ , differs at only  $1.4\sigma$  confidence from the low- $z$  reference sample ratio of  $2.1 \pm 0.2$ . AD's ratio,  $1.1 \pm 0.2$ , differs from the the low- $z$  reference sample ratio at  $3.5\sigma$  confidence.

Despite this difference in the S0/E ratio, we stress that both classifications for CL1358+62 yield fractions of early types (E+S0),  $\sim 72\%$ , and late types (S),  $\sim 28\%$ , that are identical within the errors to the low- $z$  reference sample. We can therefore draw a robust conclusion from the two sets of morphological classifications: CL1358+62 does not contain an elevated population of spiral galaxies compared with low  $z$  reference clusters. This contrasts with the results of Andreon, Davoust & Heim (1997) and and Couch et al. (1998) for other intermediate  $z$  clusters. Our work suggests that the early type/spiral classifications are likely to be secure, implying that the populations of intermediate  $z$  clusters vary significantly, even after accounting for the effects of the low  $z$  morphology-density relation.

This conclusion about the spiral population in CL1358+62 limits the range of physical models for evolution in CL1358+62, even allowing for our uncertainty about the E/S0 classifications. As we mentioned earlier, the AD classifications have the strong advantage of the same classifier at low and intermediate  $z$ . However, given the different character of the low- $z$  photographic images and the intermediate- $z$  WFPC2 images, we must acknowledge the possibility of systematic, redshift-dependent classification uncertainties. Figure 1 provides some reason to be cautious about this issue. Because we do not understand in detail the reasons for the differences between the two sets of visual classifications, we cannot be positive that the two sets of classifications bound our uncertainties. However, the best we can do at present is to leave the issue of E/S0 classifications open, and to explore the consequences of both sets of classifications below.

The DF/MF/PvD classifications would imply that cluster evolution from  $z = 0.33$  to the present does not affect the cluster morphological composition or its morphology-density relation within the observed 1.4 Mpc radius aperture. Figure 9 shows this relation for CL1358+68, binning the background subtracted data to  $I=22$  ( $M_V=-18.5$ ) radially about the dominant central galaxy. Since we are looking only for radial trends, using the deeper sample is appropriate here. The average galaxy density in each of four radial bins (0–1, 1–2, 2–3, and 3–5 arcmin) is the abscissa for this histogram. The galaxy densities in Figure 9 have been normalized to a  $M_V=-20$  limit to allow comparison with the low- $z$  reference sample. We find that the morphology-density relation for CL1358+62 is indistinguishable within the errors from the low- $z$  relation (to  $\sim M_V=-20$ ) shown in Figure 3 of Dressler et al. (1997).

The AD classifications suggest an evolutionary mechanism that decreases the fraction of E's, increases the fraction of S0's, while leaving the fraction of spirals unchanged. Assuming that there is no plausible mechanism for directly converting E's into S0's, we can exclude models that transform the observed  $z=0.33$  cluster spirals into S0's without accretion of additional galaxies. In

order to transform the  $z=0.33$  AD morphological mix into the low- $z$  reference sample population while accreting the smallest number of galaxies, the cluster population would increase by 50%. Approximately 70% of the accreted galaxies would become S0's by the present day, and 30% spirals.

## 5. The Morphological-Spectral Connection

While a great deal has been learned about the galaxy population in intermediate redshift clusters from relatively small samples of spectra, we must remember that even present-day clusters of galaxies are a heterogeneous group, differing widely in their degree of virialization. Because cluster relaxation may drive galaxy evolution, the range in cluster galaxy populations may be large at any redshift. For this reason, it is desirable to connect the morphological and spectral properties of a large sample of galaxies in each of a number of clusters directly.

We have spectral classifications from Fisher et al. (1998) sorting each of the galaxies with spectra into one of the four categories: (1) absorption lines only, (2) emission lines present, (3) emission lines plus strong Balmer absorption lines, and (4) k+a (also called E+A). Category (4) contains galaxies with the normal absorption lines of E/S0 galaxies plus strong Balmer absorption lines. Emission line galaxies have [OII] 3727 Å emission with equivalent width (EW)  $>5$  Å. If  $H_\delta$  absorption of  $>4$  Å EW is detected for an emission line galaxy, the galaxy is classified as emission plus Balmer lines. Galaxies with  $[(H_\delta + H_\gamma + H_\beta)/3]$  EW greater than 4 Å, but [OII] emission with  $<5$  Å EW, are classified as k+a. We refer the reader to Fisher et al. (1998) for a more complete summary of the spectral properties of these galaxies and a comparison with spectra of low- $z$  galaxies. Table 4 and Figure 10 summarize the comparison between the spectral and morphological properties for the 191 cluster members in common with Fisher et al. (1998), using the DF/MF/PvD classifications.

In rough terms, the bulk of the CL1358+62 galaxies follow the morphological-spectral correlation expected for bright field galaxies at low redshift: the preponderance of the E and S0 galaxies have pure absorption line spectra, while the fraction of galaxies with emission lines rises for the late type spirals. Dressler et al. (1999) found a similar behavior for galaxies in the MORPHS sample; see also Poggianti (1999). We do know, however, that the percentage of galaxies with emission lines and strong Balmer absorption lines,  $\sim 19\%$ , is higher than the  $\sim 6\%$  content of these galaxies in comparable low  $z$  clusters (Dressler (1987), see also Fisher et al. (1998)).

If we use the AD classifications for the CL1358+62 galaxies, these conclusions do not change significantly. The most interesting difference between the two sets of morphological classifications is that DF/MF/PvD classify all the E+A galaxies as types S0 to Sb, while AD classifies these galaxies as having a wider range of morphologies from E to Sbc.

## 6. Discussion and Conclusions

For CL1358+62, we have acquired a unique data set including a large mosaic of HST fields and extensive spectroscopy that allows us to unambiguously determine cluster membership for

galaxies with  $M_V < -20$ . We have directly compared the morphological classifications of two sets of classifiers for the galaxies in CL1358+62. The two sets of classifiers agree that (to a limit of  $M_V = -20$ ) the fraction of early type galaxies (and therefore spirals) in this cluster at  $z=0.33$  is indistinguishable from the fraction in comparable low- $z$  clusters. In contrast, previous workers, Andreon, Davoust & Heim (1997) and Couch et al. (1998), who also studied WFPC2 images of clusters at  $z \sim 0.3$ , found an elevated population of spirals compared with low- $z$  reference samples. Because our work confirms the reliability of early-type/spiral classifications from intermediate  $z$  WFPC2 observations, we conclude that this is evidence for a dispersion in the evolution of intermediate- $z$  clusters.

The two groups of classifiers differ on ratio of E to S0 galaxies in CL1358+62. DF/MF/PvD find a population of S0 galaxies ( $S0/E = 1.6 \pm 0.3$ ) that is within  $1.4\sigma$  of the low- $z$  reference sample, while AD finds a significantly smaller ratio ( $1.1 \pm 0.2$ ). This systematic difference is most likely related to the fact that the transition between S0's and intermediate luminosity E's is rather gradual. Many of the intermediate luminosity E's are thought to have disks, e.g. Scorz et al. (1998), Rix & White (1990), and Jorgensen & Franx (1994). It may only be possible to resolve this issue by direct model fitting to images at low and intermediate  $z$ .

Even though we conclude that we have not reliably determined the ratio of S0's to E's among the early types, our work significantly restricts possible evolutionary models. If we accept the MF/DF/PvD classifications, evolution must preserve the fraction of E's, S0's and S's as well as the morphology-density relation. If the AD classifications are correct, evolution must decrease the fraction of E's and increase the fraction of S0's while maintaining the fraction of S's. A possible mechanism for driving the evolution of the morphological mix in this latter fashion is accretion of additional galaxies from the spiral-rich infall region that become predominantly S0's. The cluster population within an  $\sim 1$  Mpc radius must increase by a minimum of 50% from  $z=0.5$  to the present day in order convert an intermediate  $z$  population rich in E's to a low- $z$  population rich in S0's. It will be interesting to see whether such accretion can be produced in simulations of cluster formation. In most cluster formation scenarios, massive clusters form by the merging of pre-existing massive clusters with (presumably) similar populations of early type galaxies. It may therefore be difficult to double the ratio of S0 to E galaxies.

We compare our morphological classifications to our previous spectral classifications and conclude that the morphologies of the spectrally “active” galaxies are as might be expected from the low- $z$  field population: the galaxies with emission lines are predominantly spirals and the k+a (or E+A) post-starburst galaxies are typically early type disk galaxies (S0–Sb).

We wish to acknowledge the generous contributions of Alan Dressler to this paper, including his independent classifications and insightful comments. We thank Gus Oemler for checking the classifications and for thoughtful comments on the manuscript, which led to several improvements. We thank Margaret Geller for a critical reading of an earlier version of the manuscript and helpful comments. Our referee, Ian Smail, and our editor, Greg Bothun, both made insightful comments that helped us clarify the paper.

## APPENDIX SYSTEMATIC EFFECTS OF MEASUREMENT ERRORS

The effects of classification errors on the distribution of types can be important. Quantifying these effects is difficult because morphological classification is a subjective procedure, but we can gain some insight by considering simple models for the errors. We begin by assuming that the numerical type is based on a one dimensional measurement with a simple, constant error. This simple model would imply that any peaks in the distribution of types would be softened. If we adopt nominal intrinsic fractions of S:S0:E of 0.20:0.53:0.27, as is approximately correct for the inner 600 kpc of low redshift clusters (Dressler et al. (1997)), the errors will automatically decrease the fraction of S0's, and enhance the fraction of E's and S's.

We can calculate an upper limit to the loss of S0's for our nominal 20:53:27 (S:S0:E) population with this model for the errors. We assume that the types are scattered with a mean absolute deviation (MAD) of 1, and all intermediate types are divided equally between adjacent types. The outcome of this experiment is a distribution of 0.27:0.38:0.34 (S:S0:E). In this case, all galaxies scattered beyond the normal type boundaries were assigned to the boundary type (i.e. E). A MAD of 1 may be an overestimate as the difference in the types assigned by the two groups of classifiers is of this order. The intrinsic errors are  $\sqrt{2}$  smaller if the errors are independent. For these smaller errors the resulting distribution would be 0.24:0.43:0.33 (S:S0:E). In either case, the results serve to illustrate that the systematic effects can be very significant.

Let us consider a second, more physical model for the visual classification errors. Here, we assume that morphological type is based on two independent variables with continuous distributions: bulge-to-total light fraction ( $f_b$ ), and asymmetric features due to spiral arms ( $A$ ). This is very similar to the quantitative classification devised by Abraham et al. (1996). Galaxies with low  $A$  will be classified as early type ( $t < 0$ ) and then divided into E's or S0's based on whether  $f_b$  is above or below a critical value. It has been argued that most  $L^*$  ellipticals have faint disks, e.g. Rix & White (1990) and Jorgensen & Franx (1994). Similarly, the spiral classification will be based on a combination of  $f_b$  and  $A$ .

If the intrinsic distribution of  $f_b$  is flat, then errors in  $f_b$  will not change the ratio of S0's to E's. However, if the intrinsic distribution of  $f_b$  is peaked, the errors will have a systematic effect. The sign depends on the details of the intrinsic  $f_b$  distributions and the size of the errors. Contributing to this uncertainty, the errors can also be asymmetric, if for example, faint extended disks are missed in noisy data. The situation is similar for errors in  $A$ , where E's and Sa's now share a boundary. Extensive simulations are required to estimate the systematic effects of limited S/N on classification errors, taking into account the the point spread function of WFPC. We will undertake this effort in a future paper.

## REFERENCES

Abraham, R. et al. 1996, ApJS, 107, 1.  
Andreon, S., Davoust, E. & Heim, T. 1997, A&A, 323, 337.

Andreon, S. 1998, *ApJ*, 501, 533.

Andreon, S. et al. 1996, *A&AS*, 116, 429.

Bertin, E. & Arnouts, S. 1996, *A&A*, 117, 393.

Butcher, H. & Oemler, A.. 1984, *ApJ*, 285, 426.

Couch, W. & Sharples, R. 1987, *MNRAS*, 229, 423.

Couch, W. et al. 1998, *ApJ*, 497, 188.

Dressler, A. 1980, *ApJ*, 236, 351.

Dressler, A. 1987, *Nearly Normal Galaxies*, ed. Faber, S., (New York:Springer-Verlag), 276.

Dressler, A. & Gunn, J.E. 1992, *ApJS*, 78, 1.

Dressler, A. et al. 1997, *ApJ*, 490, 577.

Dressler, A. et al. 1999, *ApJS*, 122, 51.

Fabricant, D., McClintock, J. & Bautz, M. 1991, *ApJ*, 381, 33.

Fisher, D., Fabricant, D., Franx, M., & Van Dokkum, P. 1998, *ApJ*, 498, 195.

Frei, Z. & Gunn, J. 1994, *AJ*, 108, 1476.

Geller, M. et al. 1997, *AJ*, 114, 2205.

Griffiths, R. et al. 1994, *ApJ*, 435, L19.

Gunn, J. & Dressler, A. 1988, *Towards Understanding Galaxies at High Redshift*, ed. Kron, R. & Renzini, A., (Dordrecht:Kluwer), 227.

Holtzmann, J. et al. 1995, *PASP*, 107, 156.

Jansen, R. et al. 1999, submitted to *ApJ*.

Jorgensen, I. & Franx, M. 1994, *ApJ*, 433, 553.

Kelson, D. et al. 1997, *ApJ*, 478, 13.

Kennicutt, R. C., Jr. 1992, *ApJ*, 388, 310.

Lubin, L. et al. 1998, *AJ*, 116, 584.

McLeod, B. & Rieke, M. 1995, *ApJ*, 454, 611.

Morgan, W. W. & Mayall, N. U. 1957, *PASP*, 69, 291.

Morgan, W. W. & Osterbrock, D. E. 1969, *AJ*, 74, 515.

Poggianti, B. M. 1997, *A&AS*, 122, 399.

Poggianti, B. M. 1999, *ApJ*, 518, 576.

Postman, M. et al. 1998, *ApJ*, 506, 33.

Ratnatunga, K., Griffiths, R., & Ostrander, E. 1999, *AJ*, submitted.

Rix, H.-W. & White, S. 1990, *ApJ*, 362, 52.

Sandage, A. 1961, *The Hubble Atlas of Galaxies* (Washington, DC: Carnegie Institution of Washington)

Sandage, A. & Tammann, G. A. 1987, *A Revised Shapley-Ames Catalog of Bright Galaxies* (Washington, DC: Carnegie Institution of Washington)

Scorza, C. et al. 1998, *A&AS*, 131, 165.

Shectman, S. et al. 1996, *ApJ*, 470, 172.

Smail, I. et al. 1997, *ApJS*, 110, 213.

van Dokkum, P. et al. 1998, *ApJ*, 500, 714.

Table 1. Combination Rules for Morphological Types

Classifier 1	Classifier 2	Classifier 3	Final Classification
-5	-5	-4	-5
-5	-5	-2	-4
-5	-4	-4	-4
-5	-4	-2	-4
-4	-4	-2	-4
-2	-2	-5	-4
-2	-2	-4	-2
-2	-2	0	-2
-2	-2	1	0
-2	-2	2	0
-2	0	1	0
-2	1	1	0
-2	1	2	0

Note. — These rules are used to assign morphological types if the three authors did not agree exactly. If the classifications span five numerical types or less between 0 and 10, the three numbers are averaged. The average is rounded up or down to the nearest whole numerical type. If the classifications span more than five numerical types, but all are between 1 and 99, we assign type 15. Note that the order of the authors is not significant.

Table 2. Morphological Catalog for CL1358+62

Number	X	Y	I	cz	Type (DF/MF/PvD)	Type (AD)
1	2185.23	198.20	20.85	99246	-4	-4
12	4165.23	344.75	19.79	97702	-2	-4
15	3424.60	366.51	19.24	95807	-2	1
16	2155.44	387.90	19.36	97243	1	1
25	968.84	444.59	20.54	129864	6	5
27	4576.15	456.72	19.00	-	5	5
30	1479.89	477.46	19.38	98463	-4	-5
33	4231.61	489.34	19.13	143869	0	0
35	4095.85	492.36	20.47	98424	-4	-3
37	3526.59	495.73	20.42	96743	-2	-2
38	3377.31	502.24	18.81	99803	0	-2
48	3302.50	558.38	20.98	164142	15	99
51	4062.30	568.56	20.77	-	8	4
52	3024.67	571.39	16.96	48524	4	3
53	3081.65	574.07	20.08	-	4	5
54	1525.88	580.51	15.69	25570	4	5
61	2357.29	602.25	20.50	144702	15	7
66	4121.06	625.81	20.99	-	-2	-2
68	3470.13	635.49	18.95	96710	-2	-2
70	3598.20	642.90	20.04	80512	5	5
79	4072.28	697.05	18.92	98334	0	-4
94	2580.14	725.66	19.64	97702	-2	-2
101	2602.51	739.65	20.44	151970	0	-5
103	3652.82	740.90	20.43	95699	3	5
107	3499.88	757.63	20.99	-	4	5
114	2736.96	794.55	18.89	31012	5	6
118	2286.07	807.47	19.08	97741	0	-1
120	1458.64	807.67	20.02	-	6	5
125	4464.63	814.64	20.65	-	5	5
127	3372.60	818.52	19.95	99845	-4	-5
132	907.72	840.09	20.65	-	-5	-5
140	1319.17	854.62	19.83	98991	-4	-5
156	1940.02	919.07	19.74	149319	1	99
159	3641.99	927.73	20.65	-	5	4
162	2605.02	933.83	19.94	-	99	-3
178	558.31	1001.72	20.38	-	999	99
180	1745.41	1004.04	18.59	96677	0	1
186	2657.55	1009.86	20.83	-	-5	-5
192	3689.81	1034.60	20.64	100272	-2	-2
197	2634.39	1041.72	19.94	144632	2	2

Table 2—Continued

Number	X	Y	I	cz	Type (DF/MF/PvD)	Type (AD)
205	1501.76	1068.61	19.61	120912	5	1
206	3733.06	1075.41	20.86	98397	0	0
222	873.00	1136.15	20.86	99237	-4	-5
237	2777.48	1171.76	19.64	97525	5	3
239	1674.39	1188.96	20.92	207514	7	10
244	3455.89	1200.72	20.08	-	999	999
248	1019.98	1207.10	20.02	99291	-2	-2
269	698.78	1258.32	20.54	-	4	6
277	1244.07	1269.37	20.59	-	2	2
279	999.08	1272.41	20.44	162101	4	3
283	1400.74	1280.19	20.93	98430	-2	-2
285	3410.44	1288.24	20.66	100257	4	4
286	2933.14	1291.02	20.34	98343	6	4
295	1818.09	1320.64	17.85	25606	4	3
299	2669.82	1334.75	18.88	100970	0	-2
303	3046.19	1343.52	19.71	97417	-2	-2
304	4330.18	1348.34	17.29	23213	1	1
314	1730.45	1364.59	20.88	97564	-2	-2
316	1147.10	1373.25	20.47	99893	0	3
325	946.39	1406.99	19.25	96686	-5	-5
326	3531.82	1407.04	20.77	100281	-2	0
327	3089.78	1412.64	19.03	99330	1	1
328	1340.92	1417.67	20.94	202745	0	3
331	3058.10	1427.59	19.08	98481	-2	-2
333	4153.37	1437.70	18.87	98104	-5	-5
336	3083.01	1446.02	19.79	97627	-2	-2
338	2994.05	1447.54	20.62	-	2	1
352	869.48	1493.94	20.70	45442	3	3
362	715.38	1525.08	20.21	99597	1	1
368	2960.35	1547.05	19.92	99513	0	0
382	697.67	1576.68	20.71	149212	6	5
385	1150.11	1586.52	18.25	98976	-4	-5
392	3917.25	1608.25	18.60	98541	3	3
393	2331.21	1609.32	20.61	99237	-2	-2
397	2423.80	1617.24	19.02	100430	-2	-2
399	765.00	1624.56	20.76	159692	0	-2
415	2527.55	1680.94	19.65	98682	-4	-5
433	2519.00	1709.59	21.00	-	6	4
434	2712.22	1710.19	18.44	97642	-5	-5
435	1048.97	1710.26	20.02	190882	3	2

Table 2—Continued

Number	X	Y	I	cz	Type (DF/MF/PvD)	Type (AD)
442	2657.45	1722.45	20.88	98607	1	-2
452	3575.83	1753.56	19.99	98086	1	0
457	2202.26	1758.15	19.29	98688	-2	-3
468	2524.04	1780.65	20.30	170632	2	1
476	2164.48	1808.28	18.87	96773	-4	-5
484	2281.67	1835.66	17.57	97168	-5	-5
496	4657.77	1869.51	20.93	-	-4	-5
499	926.31	1877.15	19.85	160364	-5	-5
513	3385.76	1937.13	19.49	99860	0	-2
519	2633.79	1953.48	17.76	98691	-4	-5
520	2267.84	1953.77	19.98	98961	-5	-5
521	2598.87	1954.62	20.06	99504	-2	-2
526	1819.56	1976.82	20.91	-	-4	-5
529	2019.97	1981.74	20.50	118028	15	-3
530	2604.02	1985.11	19.63	99198	-2	-2
533	3492.41	1992.67	19.56	97120	-5	-5
541	2558.48	2016.50	20.55	-	0	1
545	1341.00	2022.51	20.10	149243	0	-4
546	4213.68	2023.37	17.26	23768	5	4
550	2819.78	2034.77	20.70	100970	1	0
558	2046.76	2042.20	19.76	95753	-2	-2
559	4563.94	2045.51	20.58	-	4	4
561	4130.90	2050.21	19.46	207072	15	99
562	2886.03	2061.80	18.43	69161	4	3
563	2957.63	2065.25	20.21	100760	6	0
564	3187.62	2070.07	19.06	97222	0	-2
570	3067.16	2074.98	20.66	99522	-2	-5
581	2750.58	2107.99	19.12	98421	-2	-2
591	2604.10	2133.40	18.36	97762	-2	-2
602	2350.33	2175.38	20.38	94464	-5	-5
606	2651.60	2182.44	19.05	96413	-2	-4
611	1909.12	2186.08	18.89	97612	-5	-5
623	4308.50	2227.50	19.93	99776	3	2
624	2123.91	2231.85	19.46	52634	0	-3
629	5040.18	2242.21	17.88	76299	4	1
636	2538.86	2258.28	18.75	97342	-4	-5
639	2777.26	2264.35	20.40	98032	-2	-2
641	4305.25	2279.18	20.95	23920	6	4
643	2833.92	2289.38	20.50	148539	-2	-2
647	2897.12	2311.32	20.21	-	6	5

Table 2—Continued

Number	X	Y	I	cz	Type (DF/MF/PvD)	Type (AD)
651	3624.13	2320.14	21.00	100652	-2	-1
653	3096.27	2325.88	19.87	100251	-2	-4
655	4925.76	2334.26	20.04	98116	-2	-2
656	3032.45	2336.55	20.17	99708	-2	-2
662	2762.21	2350.96	19.15	95205	1	1
663	2002.63	2352.95	20.24	83425	0	-5
670	4792.86	2365.01	19.75	98125	-2	-2
679	2891.70	2395.08	19.51	96653	0	-5
680	4456.98	2396.53	20.87	124924	2	3
685	4144.73	2406.59	20.20	-	-4	-5
698	2673.91	2444.21	20.95	-	3	4
707	3017.95	2463.86	20.54	-	0	-2
711	2158.68	2471.78	19.83	96536	-2	-5
712	2420.36	2476.45	19.69	99920	0	1
713	2213.24	2477.51	20.55	-	5	4
717	2719.31	2486.68	18.78	96452	-2	-2
719	2172.06	2489.81	20.78	99339	-5	-5
724	2281.36	2494.96	18.85	98302	-5	-5
730	1712.08	2511.63	19.03	99830	3	1
732	2705.21	2518.39	20.23	96773	-2	-2
736	3434.65	2523.63	20.51	98451	0	0
743	2741.21	2541.98	20.06	98272	-5	-5
745	2878.57	2542.91	17.95	97033	-4	-5
748	2835.90	2554.58	20.25	97048	-5	-5
767	2784.63	2608.14	19.91	98302	-5	-5
768	2566.24	2608.94	18.44	101929	1	1
771	2851.49	2618.35	19.79	97462	-5	-2
774	3465.80	2625.73	18.81	97342	-2	-5
775	2818.67	2625.80	19.50	96824	-5	-5
778	3368.31	2635.15	20.05	99351	1	1
793	4179.71	2668.46	19.19	97036	-4	-2
794	2810.14	2668.81	19.23	98514	2	1
799	4028.08	2680.53	19.29	96161	0	-4
801	1766.29	2685.75	18.63	96038	1	2
803	3671.86	2687.29	18.34	99702	1	0
810	2801.93	2719.27	17.11	98182	-5	-5
813	3341.70	2731.51	19.51	96383	-2	-2
822	4639.03	2748.37	19.05	96997	5	6
828	2521.07	2770.37	19.91	97912	6	6
831	2801.07	2781.44	18.74	97672	-4	-5

Table 2—Continued

Number	X	Y	I	cz	Type (DF/MF/PvD)	Type (AD)
838	2248.16	2789.85	20.14	-	999	-5
842	2906.30	2794.44	20.39	100670	999	0
843	4713.68	2796.95	20.55	48385	7	7
846	2774.56	2803.87	19.72	96563	-5	-5
867	2612.37	2853.73	18.37	97042	-4	-2
872	3640.91	2868.48	20.90	-	-2	-1
877	1235.86	2875.59	20.67	121526	1	0
886	2138.47	2909.08	20.20	95723	8	9
887	1185.86	2912.30	20.47	-	999	999
888	1978.03	2915.65	19.48	96563	0	-2
889	3904.51	2916.67	20.36	97801	0	1
890	3514.41	2918.22	20.68	97564	-4	-2
898	3185.08	2942.27	20.62	-	-5	-1
900	3332.43	2943.17	20.63	97732	-2	-2
905	1591.54	2966.15	20.91	98451	-5	-5
909	3911.90	2973.01	20.31	187822	1	1
912	1895.44	2979.65	20.09	98751	-5	-3
913	2748.21	2980.39	19.26	95816	-2	-2
922	3294.59	3021.22	19.65	98931	-2	-2
927	2019.29	3026.93	19.25	95274	-5	-5
929	3951.51	3033.18	20.10	96263	0	-1
933	4515.25	3035.84	19.87	-	-4	-5
938	1691.42	3049.42	19.25	71440	-4	0
942	2829.86	3058.61	20.59	96428	-2	-5
943	3816.51	3058.75	19.94	-	-2	-2
944	2420.93	3065.24	20.94	-	-5	-5
948	4108.78	3075.68	20.49	-	-5	-4
961	2478.92	3095.09	19.79	99381	-5	-5
967	3606.49	3104.33	20.10	-	4	1
971	3131.00	3106.51	19.94	47565	5	3
975	3024.81	3120.83	20.95	-	99	99
978	2832.26	3123.45	20.24	-	-4	-5
993	3323.02	3154.25	19.05	97735	0	-1
1003	2815.02	3176.78	20.76	100763	-5	-5
1012	2910.90	3204.76	20.77	-	-2	-4
1019	1598.82	3220.61	20.02	98718	0	1
1020	2661.84	3222.75	18.46	83578	3	1
1027	2954.26	3244.74	20.28	96686	0	-2
1036	4346.84	3277.98	19.22	99165	-2	-2
1041	4453.92	3289.61	19.78	98649	-2	-2

Table 2—Continued

Number	X	Y	I	cz	Type (DF/MF/PvD)	Type (AD)
1042	3771.63	3293.33	20.93	-	-2	1
1045	4485.09	3295.86	19.95	44686	99	99
1049	2469.20	3302.45	20.58	-	0	0
1062	3268.23	3338.69	18.84	98182	0	-1
1064	4749.89	3342.41	19.45	96182	5	2
1069	1366.71	3359.61	19.95	99060	0	-2
1075	4869.37	3367.38	19.90	62244	1	-2
1080	2041.26	3397.59	20.86	98421	-5	-5
1091	3315.98	3426.51	20.51	99579	-2	0
1100	4416.75	3462.54	20.73	159095	15	99
1105	2881.63	3475.46	18.79	98323	-2	-2
1108	2836.73	3485.88	19.42	99081	1	-1
1121	1960.44	3512.66	20.68	-	-4	-5
1127	2942.66	3523.15	20.76	159362	5	3
1141	4517.75	3545.75	19.93	99657	-2	-2
1146	4117.26	3561.40	18.27	100080	-5	-5
1153	2566.37	3583.80	20.14	61935	9	99
1157	2487.08	3591.79	18.64	62207	9	5
1158	3279.02	3592.19	20.16	99935	-2	-2
1161	2923.10	3597.44	20.01	-	-5	-5
1163	1348.04	3601.03	20.12	144364	1	3
1177	2091.53	3633.12	20.39	216269	15	1
1178	2361.82	3635.18	20.30	99234	-2	-1
1192	3212.40	3665.38	20.39	97375	-5	-5
1200	2024.55	3679.35	20.59	-	5	7
1207	3978.09	3693.67	20.68	100221	-4	-2
1209	3395.58	3703.43	19.10	83882	1	1
1211	2923.22	3706.89	20.79	99177	-4	-5
1214	3909.03	3714.53	19.51	100323	1	1
1223	2310.92	3752.63	20.49	-	-5	-5
1231	3481.26	3785.53	20.32	99018	-2	0
1235	2884.78	3791.48	20.67	-	-4	-2
1239	2759.52	3812.84	20.00	62264	3	2
1240	2878.69	3813.83	20.24	122164	4	7
1253	995.43	3851.25	19.37	97093	2	4
1255	2908.32	3863.10	20.54	-	0	3
1258	2180.86	3869.70	20.60	-	-5	-5
1265	3358.24	3888.19	19.60	99896	-2	-2
1272	3738.88	3907.25	20.85	99501	-2	-1
1273	2182.60	3907.71	20.83	-	-5	0

Table 2—Continued

Number	X	Y	I	cz	Type (DF/MF/PvD)	Type (AD)
1275	2223.31	3912.98	20.08	99141	-2	-1
1285	1476.03	3937.66	19.84	188687	1	1
1287	2727.83	3947.24	20.20	-	-2	-2
1297	2476.43	3965.12	20.88	97102	-2	-2
1298	2291.46	3965.96	20.79	-	-2	-2
1299	1553.40	3967.72	20.25	98964	3	3
1301	1428.04	3978.07	19.40	99342	0	-2
1303	3180.35	3982.62	18.98	96901	0	-2
1308	1799.52	3992.55	20.30	-	5	3
1322	1469.20	4032.65	20.90	-	-2	-2
1330	2626.63	4050.56	19.91	97051	15	10
1335	3007.32	4063.99	20.39	-	-4	-4
1343	2119.25	4082.59	17.77	99156	-5	-5
1357	1560.05	4129.23	19.78	97000	-5	-2
1367	2972.68	4167.09	18.02	98299	-5	-5
1370	3118.58	4169.24	19.71	97738	-2	-5
1372	3911.67	4178.76	20.50	98472	-5	-5
1374	3888.45	4183.67	20.52	97699	-2	-2
1376	3489.91	4187.61	19.91	98275	-2	-2
1377	2964.53	4192.76	19.23	97975	-5	-5
1379	3412.68	4193.30	20.93	-	0	2
1382	2988.76	4209.19	20.23	-	3	4
1387	2761.87	4222.14	19.18	99417	-5	-5
1395	848.83	4239.90	19.39	99771	-2	1
1405	3807.69	4288.35	20.12	99285	-4	-5
1409	3951.25	4295.39	19.69	54964	-2	-2
1411	2500.75	4322.96	19.74	-	999	-2
1413	3281.08	4328.24	19.37	99774	2	2
1414	1303.46	4329.27	20.65	95615	5	3
1415	288.53	4331.63	18.70	98844	-5	-5
1423	3633.52	4361.01	20.56	98799	-2	-2
1430	4193.88	4380.15	20.61	99222	999	3
1431	3125.60	4381.56	20.86	-	-2	-4
1438	574.34	4410.17	18.72	81105	2	1
1439	3020.74	4422.23	19.27	99339	0	-5
1447	755.69	4452.72	20.97	171424	3	4
1454	3375.34	4469.90	20.28	100859	-2	-3
1461	4207.84	4489.60	20.98	97279	-2	-5
1466	3188.31	4501.44	20.62	-	5	5
1481	810.82	4540.51	20.61	99791	-2	2

Table 2—Continued

Number	X	Y	I	cz	Type (DF/MF/PvD)	Type (AD)
1483	825.24	4542.01	19.36	99791	-5	-5
1488	661.75	4553.49	19.55	80904	-2	-4
1524	943.52	4664.34	20.89	190098	6	5
1529	3450.04	4681.31	20.81	114632	15	10
1540	3674.58	4731.74	18.01	21317	5	6
1541	2265.25	4732.11	20.43	98778	-5	-5
1559	3242.72	4783.73	20.72	100380	1	1
1563	4731.77	4795.22	20.88	-	-2	-1
1567	768.30	4815.43	20.88	100284	99	10
1568	4014.76	4819.25	19.46	36222	99	-5
1571	2338.11	4825.66	19.97	83803	4	5
1588	4185.04	4870.66	20.95	126167	0	-4
1594	1852.07	4887.76	19.87	-	999	999
1621	1467.74	4980.41	20.03	-	-5	999
1623	1937.90	4990.12	20.86	187086	-2	-2
1634	3158.57	5037.47	19.28	31985	9	5
1664	2256.63	5240.59	20.61	248908	5	2
1666	2243.04	5270.84	19.15	99552	1	2

Note. — We consider those galaxies with  $94318 < \text{cz} < 102532$  to be cluster members. Each pixel for the X and Y positions corresponds to  $0.1''$ , and the cluster center is taken to be coincident with the center of galaxy #810 at 2801.93, 2719.27. This corresponds to R.A. [1950]  $13^h 58^m 20^s.7$ , decl. [1950]  $62^\circ 45' 33''$ .

Table 3. Evolution of the Morphological Mix in CL1358+62 (%)

Type	CL1358 (DF/MF/PvD)	CL1358 (AD)	Low Z (AD)
E	$27 \pm 4$	$35 \pm 5$	$23 \pm 2$
S0	$44 \pm 6$	$38 \pm 5$	$49 \pm 3$
S	$29 \pm 5$	$27 \pm 4$	$27 \pm 2$

Note. — We assume that the unclassified galaxies in the CL1358+62 sample (1.5%) have the same morphological mix as the classified galaxies. The classifications for CL1358 in column 2 are the combined work of DF, MF and PvD (see text for details). The classifications in column 3 are the independent work of AD. The limiting magnitude is  $\sim M_V = -20$ , and the limiting radius is  $\sim 1400$  kpc.

Table 4. Spectral vs. Morphological Properties of Galaxies in CL1358+62

Type	Pure Absorption	Emission Lines	Emi. + Balmer Abs.	k+a
E	46	1.5	0.5	0
S0	76.5	2.5	1.5	7
Sa-Sb	26.5	5	2	4
Sbc-Irr	3	4	6	0
Merger	0	1	1	0
?	3	0	0	0

Note. — The DF/MF/PvD morphological classifications are used here; the spectral classifications are from Fisher et al. (1998). Ambiguous types (E or S0, S0 or Sa) are split equally between the two adjacent types, accounting for the fractional galaxies.

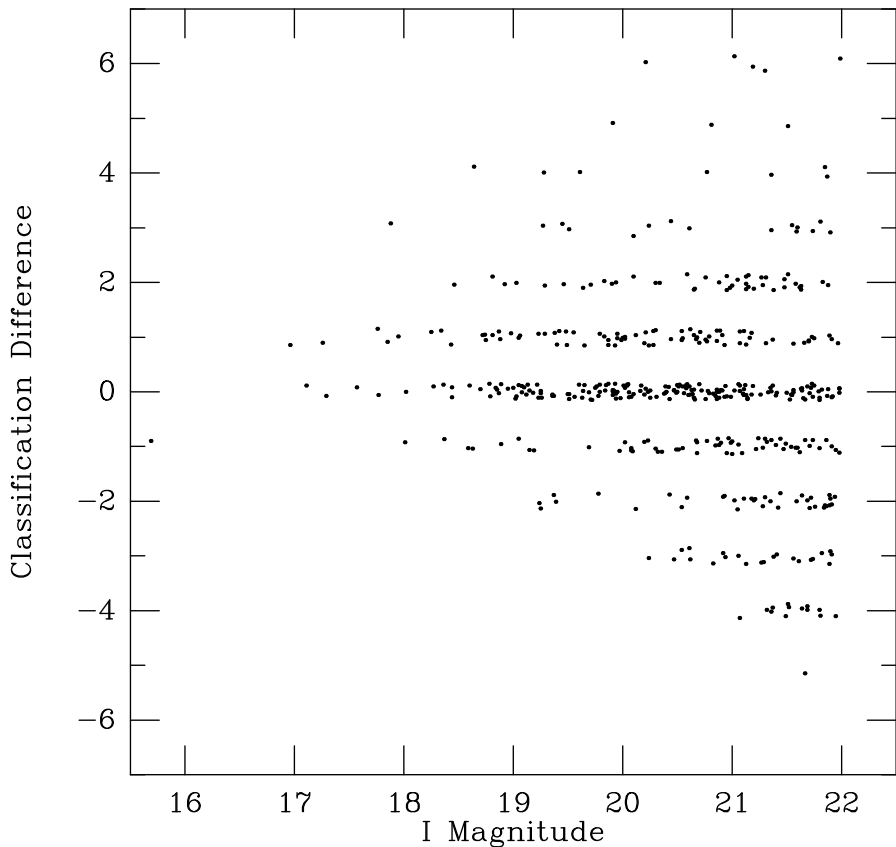


Fig. 1.— The difference between the DF/MF/PvD classifications and the AD classifications as a function of  $I$  magnitude. For the purposes of Figures 1–3 the numbers corresponding to morphological type have been shifted and condensed. For these figures, E is -3, E/S0 or S0/E is -2, S0 is -1, and S0/Sa or Sa/S0 is 0. The later morphological types have been assigned the conventional numbers described in the text. The difference between the classifications rises steeply below  $I = 22$ .

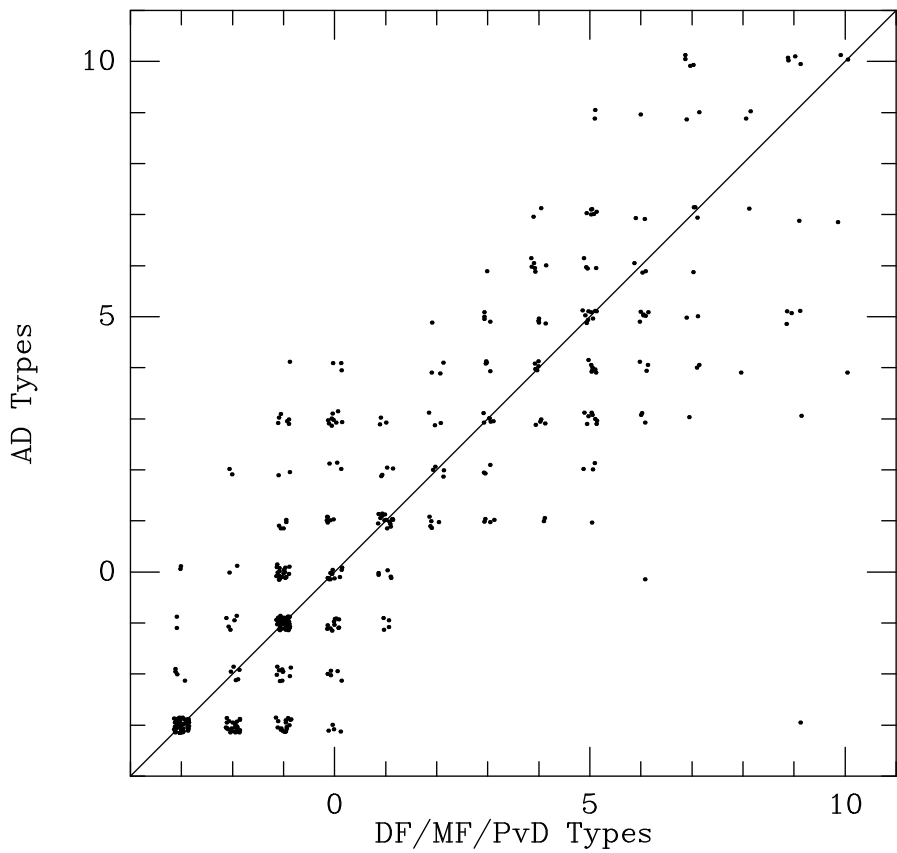


Fig. 2.— A scatter diagram comparing the two sets of classifications. See the text or the caption of Figure 1 for the conversion to morphological types.

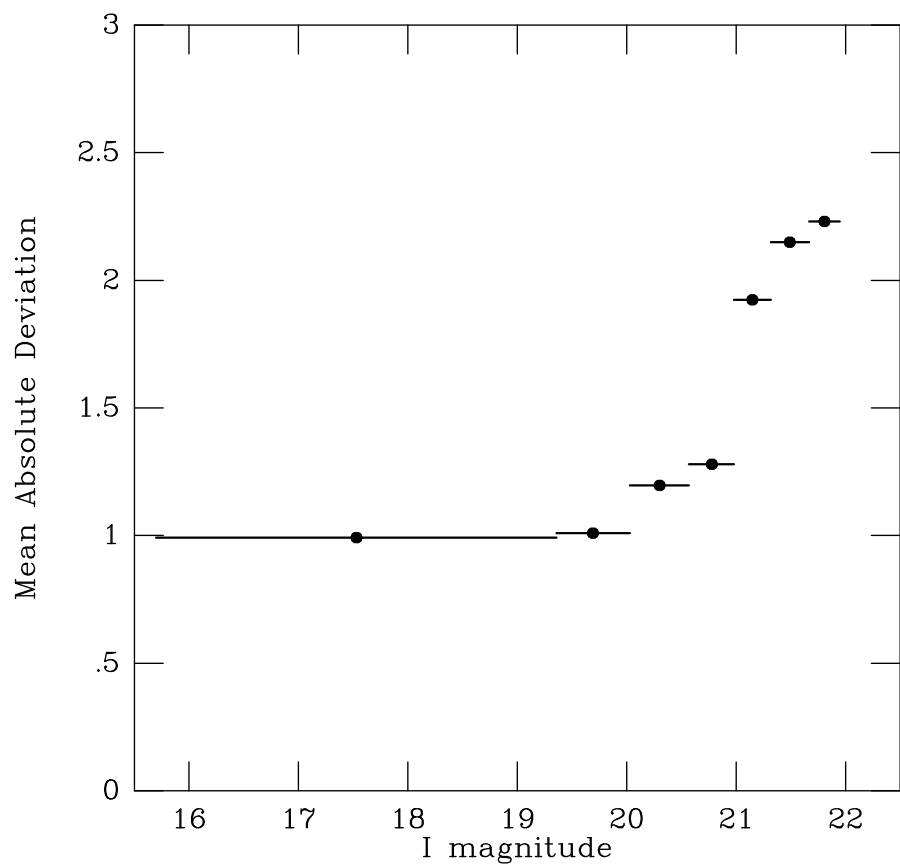


Fig. 3.— The mean absolute deviation between the two sets of classifications as a function of *I* magnitude, normalized to the mean absolute deviation of a Gaussian function with a standard deviation of 1.

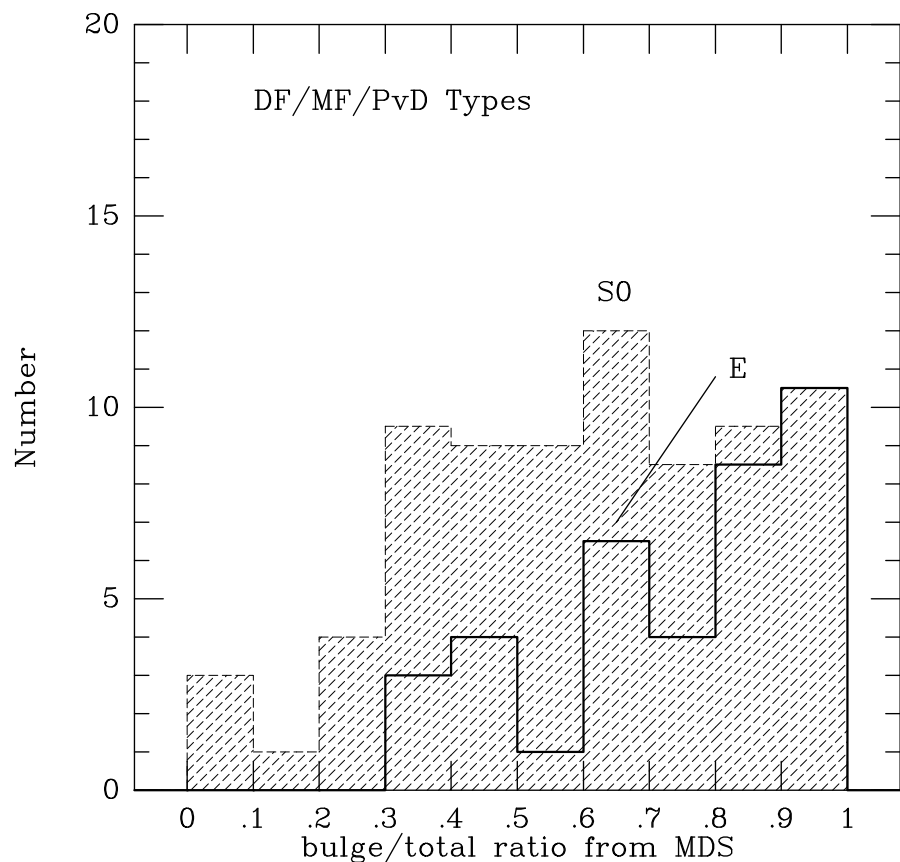


Fig. 4.— A comparison of the MDS bulge to total light ratios for galaxies that DF/MF/PvD classify as S0 and E, excluding ambiguous types -4 and 0. The magnitude limit is  $I = 21$ . MDS structural parameters are available for  $\sim 70\%$  of the CL1358+62 galaxies.

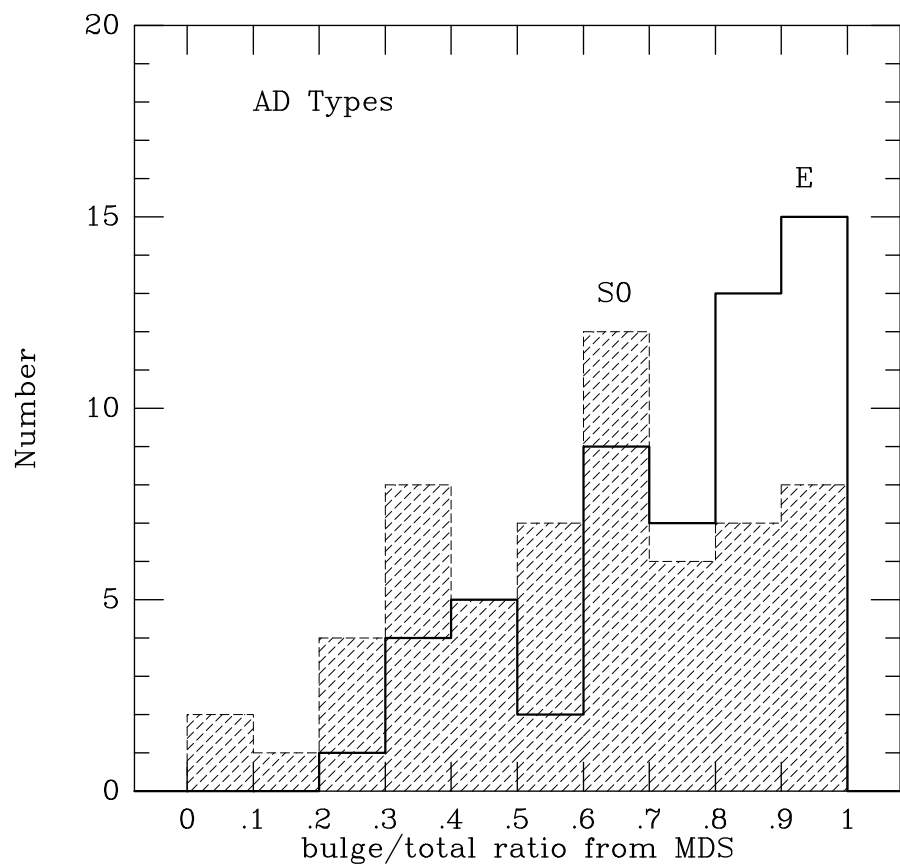


Fig. 5.— A comparison of the MDS bulge to total light ratios for galaxies with  $I < 21$  classified by AD as S0 and E.

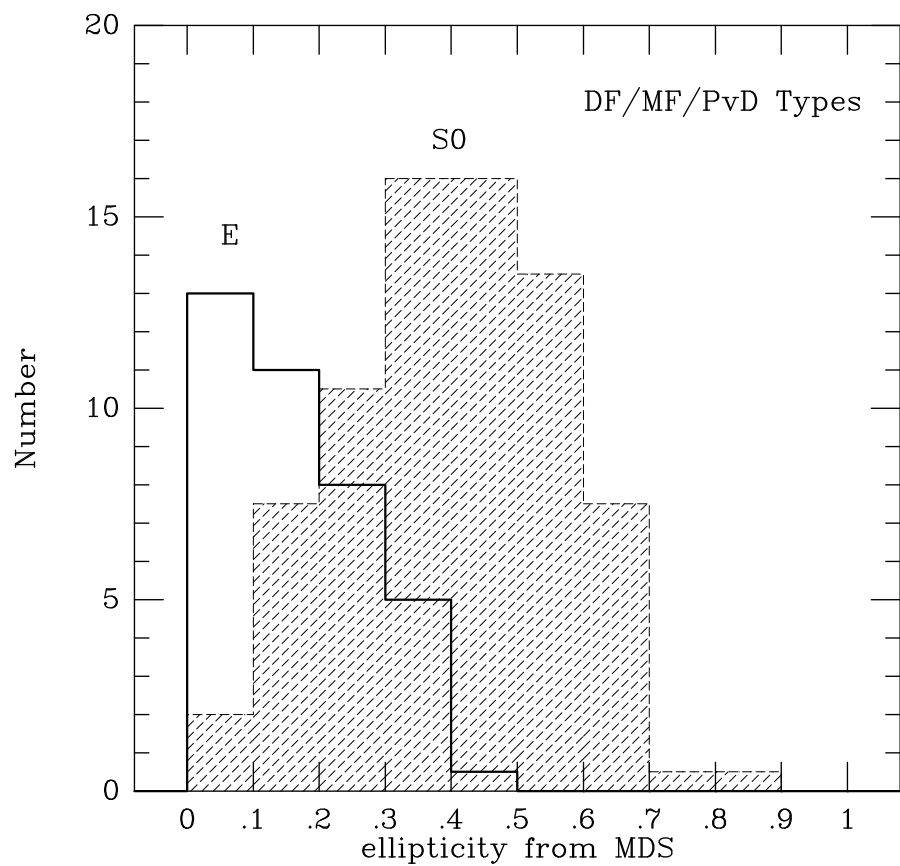


Fig. 6.— The ellipticity distributions for the galaxies with  $I < 21$  classified by DF/MF/PvD as S0 and E. Ambiguous types -4 and 0 were excluded.

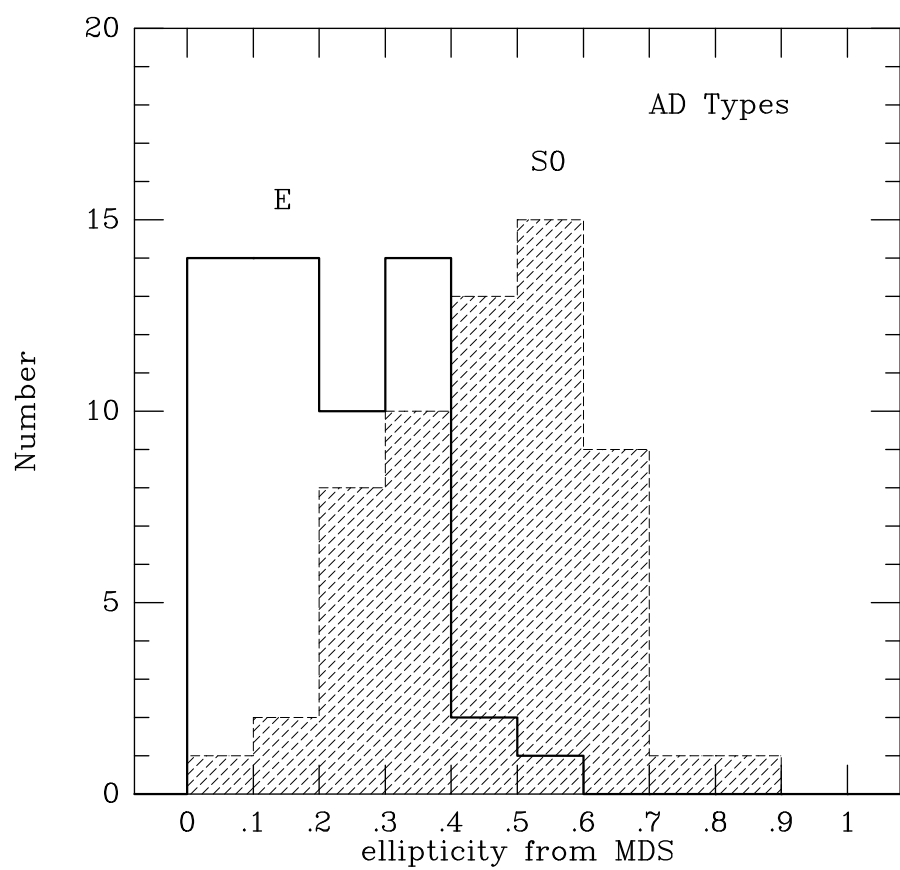


Fig. 7.— The ellipticity distributions for the galaxies with  $I < 21$  classified by AD as S0 and E.

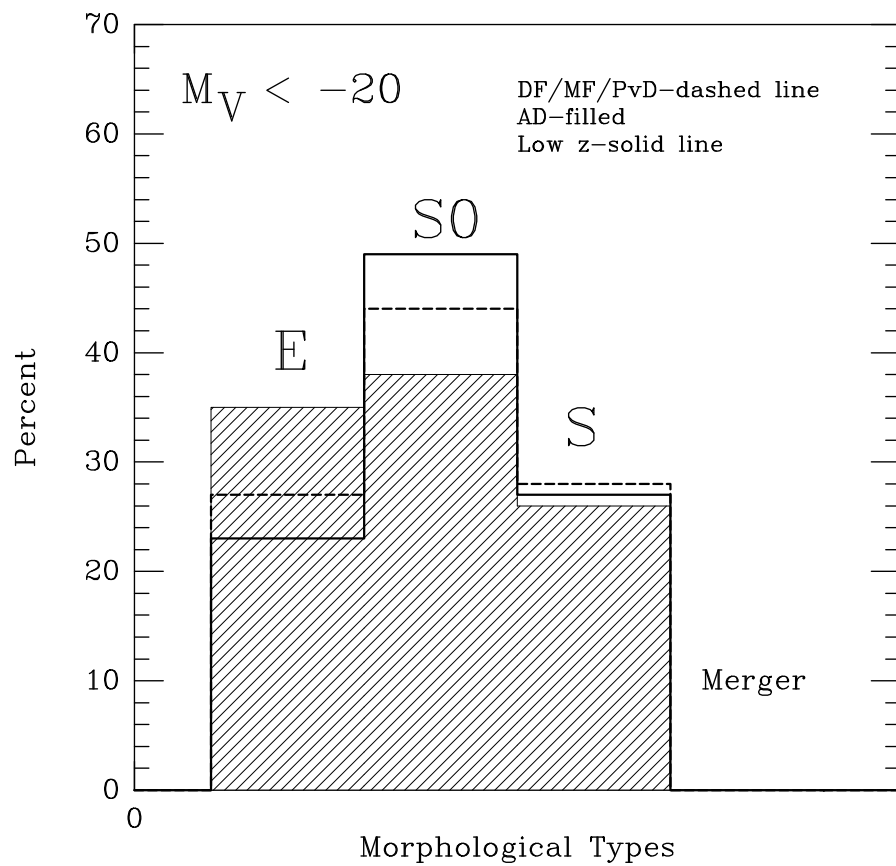


Fig. 8.— The morphological composition of CL1358+62 compared with the low- $z$  reference sample of Dressler et al. (1997). In both cases, the limiting magnitude is  $M_V \sim -20$  and the limiting radius is  $\sim 1400$  kpc. Both sets of classifications for CL1358+62 are shown.

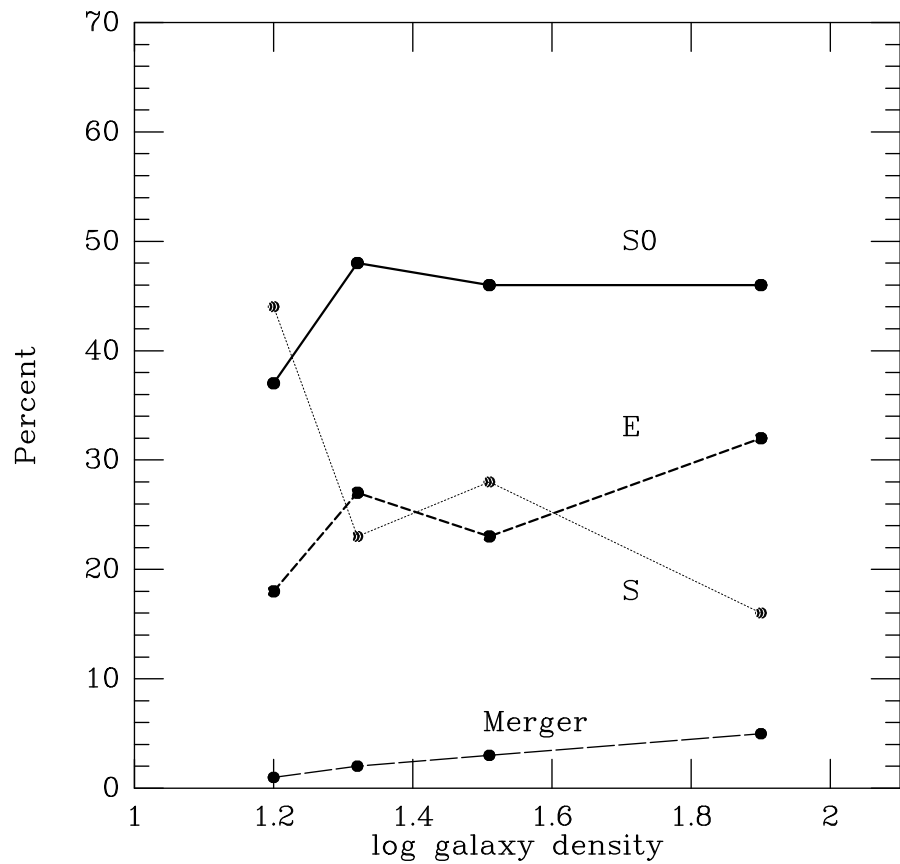


Fig. 9.— The morphology-density relation in CL1358+62 using the DF/MF/PvD classifications. This relation is almost identical to that plotted in Figure 12 of Dressler et al. (1997) for the low- $z$  reference sample.

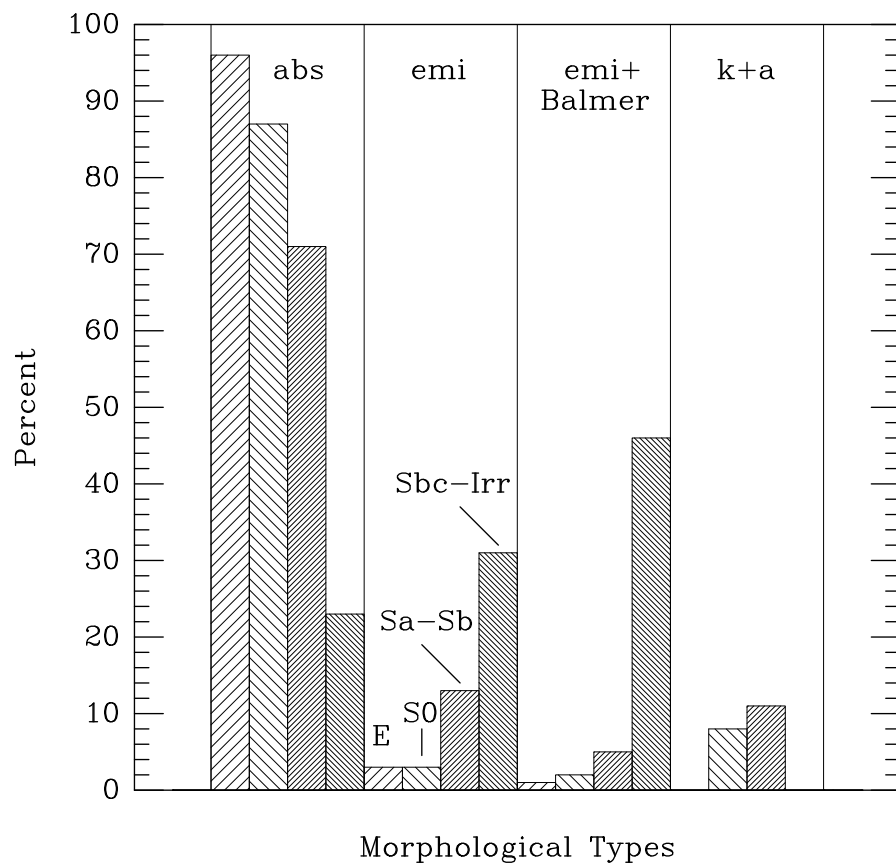


Fig. 10.— The relation between the morphological and spectral properties of the CL1358+62 galaxies, using the DF/MF/PvD classifications.